Proton Transfer Dynamics on the Surface of the Late M State of Bacteriorhodopsin

Esther Nachliel,* Menachem Gutman,* Jörg Tittor,[†] and Dieter Oesterhelt[†]

*Laser Laboratory for Fast Reactions in Biology, Department of Biochemistry, Tel Aviv University, Tel Aviv 69978, Israel; and [†]Max Planck Institut für Biochemie, Martinsried D-82152, Germany

ABSTRACT   The cytoplasmic surface of the BR (initial) state of bacteriorhodopsin is characterized by a cluster of three carboxylates that function as a proton-collecting antenna. Systematic replacement of most of the surface carboxylates indicated that the cluster is made of D104, E161, and E234 (Checover, S., Y. Marantz, E. Nachliel, M. Gutman, M. Pfeiffer, J. Tittor, D. Oesterhelt, and N. Dencher. 2001. *Biochemistry.* 40:4281–4292), yet the BR state is a resting configuration; thus, its proton-collecting antenna can only indicate the presence of its role in the photo-intermediates where the protein is re-protonated by protons coming from the cytoplasmic matrix. In the present study we used the D96N and the triple (D96G/F171C/F219L) mutant for monitoring the proton-collecting properties of the protein in its late M state. The protein was maintained in a steady M state by continuous illumination and subjected to reversible pulse protonation caused by repeated excitation of pyranine present in the reaction mixture. The re-protonation dynamics of the pyranine anion was subjected to kinetic analysis, and the rate constants of the reaction of free protons with the surface groups and the proton exchange reactions between them were calculated. The reconstruction of the experimental signal indicated that the late M state of bacteriorhodopsin exhibits an efficient mechanism of proton delivery to the unoccupied—most basic—residue on its cytoplasmic surface (D38), which exceeds that of the BR configuration of the protein. The kinetic analysis was carried out in conjunction with the published structure of the M state (Sass, H., G. Büldt, R. Gessenich, D. Hehn, D. Neff, R. Schlesinger, J. Berendzen, and P. Ormos. 2000. *Nature.* 406:649–653), the model that resolves most of the cytoplasmic surface. The combination of the kinetic analysis and the structural information led to identification of two proton-conducting tracks on the protein's surface that are funneling protons to D38. One track is made of the carboxylate moieties of residues D36 and E237, while the other is made of D102 and E232. In the late M state the carboxylates of both tracks are closer to D38 than in the BR (initial) state, accounting for a more efficient proton equilibration between the bulk and the protein's proton entrance channel. The triple mutant resembles in the kinetic properties of its proton conducting surface more the BR-M state than the initial state confirming structural similarities with the BR-M state and differences to the BR initial state.

INTRODUCTION

The photocycle of bacteriorhodopsin is one of the best-studied light-driven biochemical reactions. The mechanism is interpreted as a combination of three events: the isomerization of the retinal residue (all-*trans* to 13-*cis*), a change in the protein that alters the connectivity between the Schiff base and the bulk phase from an extracellular facing structure to a cytoplasmic connected conformation (switch), and a proton transfer reaction that is driven by a set of pK shifts that propagate along the proton-conducting channel of the protein (Dencher et al., 2000; Haupts et al., 1997; Lanyi, 1998; Lanyi and Pohorille, 2001; Oesterhelt, 1998; Brown et al., 1998).

The best-observed feature of the photocycle is the protonation state of the Schiff base and its absorption spectrum. In the protonated state, the retinal has its maximal absorption around 570 nm and it varies with the state of protonation of residues, such as D85 and D212, that are close enough to modulate the energy of the electronic transition of the chromophore. Residues that are >8–10 Å away from the Schiff base (for example, D96) are too remote and their state of protonation is measured by FTIR spectroscopy. In the de-protonated state of the Schiff base the chromophore has a maximal absorbance at ~410 nm, and the spectral difference between the various conformations of the M state are very small (Varo and Lanyi, 1990, 1991a, b; Radionov and Kaulen, 1997).

In contrast with the state of protonation of the Schiff base, conformation of the protein is more difficult to deduce and progress was gained by a variety of physical methods such as FTIR (Chon et al., 1996; Heberle et al., 2000; Kandori et al., 1999; Rödig and Siebert, 1999; Sass et al., 1997; Zscherp et al., 1999), electron spin resonance (Mollaaghababa et al., 2000; Steinhoff et al., 1999, 2000; Thorgeirsson et al., 1997; Xiao et al., 2000), proton pulse (Checover et al., 1997, 2001; Nachliel and Gutman, 1996; Nachliel et al., 1996b, 1997), and structural studies (Dencher et al., 2000; Henderson et al., 1990; Koch et al., 1991; Lanyi, 1999; Luecke et al., 1999a, b; Mueller et al., 1995; Oesterhelt et al., 2000; Pebay-Peyroula et al., 1997; Sass et al., 1998; Subramaniam et al., 1993). However, even to date, some interconnecting loops, especially of the cytoplasmic surface, are poorly resolved. The last 16–18 residues at the C′-terminal end of the protein are probably too loose to attain a coherent conformation during the crystal-

lization and have not yet been resolved. The major conformational transition associated with the photocycle coincides with the M_1 to the M_2 step, where helices G and F exercise a transmembranal motion with enhanced hydration of the protein (Oka et al., 1999; Royant et al., 2000; Varo and Lanyi, 1995; Weik et al., 1998; Xiao et al., 2000). This structural transition is possible only in the presence of free water molecules (Dencher et al., 2000); at relative humidities below 75%, e.g., 57%, the protein can release the Schiff base proton to D85, but the conformational change associated with the M_2 formation does not materialize (Weik et al., 1998).

The mechanism of proton transfer reactions between the Schiff base and its immediate acceptor (D85) and donor (D96) are well-recognized, as the reaction is spectrally detectable. The proton transfer from the Schiff base to D85 is the first step of the proton pumping machinery and appears as the replacement of the BR spectrum by that of the deprotonated one, the M state. The elimination of the negative charge of D85 drives a sequence of pK shifts leading to release of proton from the proton releasing domain, associated with E204, E194, and water molecules in their neighborhood (Brown et al., 1995; Hatanaka et al., 1996; Pfeiffer et al., 1999; Richter et al., 1996; Ruediger et al., 1997; Tanio et al., 1999). In a similar mode, the re-protonation of the Schiff base by the proton from D96 marks the M decay. Besides these two events, the intraprotein proton transfer is less recognized. The re-protonation of D96 consists of the later steps of the photocycle (Cao et al., 1991; Otto et al., 1989; Varo and Lanyi, 1991a) in a reaction that has a surprisingly slow dynamics and is regulated by the chemical potential of the water in the reaction system. The protonation of D96 necessitates a proton transfer from the nearest carboxylate, D38 (Riesle et al., 1998), which in the BR state is 11.6 Å apart, while in the M state it is closer (10.9 Å; Sass et al., 2000).

Following the re-protonation of D96, the protein reacts with the bulk phase and the process is commonly recorded as deprotonation of a pH indicator that is either soluble or bound to the protein (Checover et al., 1997, 2001; Heberle and Dencher, 1992; Heberle et al., 1993; Nachliel et al., 1996b). The re-protonation of the protein's surface with the bulk proceeds through diffusion-controlled reactions, either with free protons or with protonated buffer molecules in the bulk. The mechanism was intensively investigated by Gutman and co-workers (Checover et al., 1997, 2001; Nachliel and Gutman, 1996; Nachliel et al., 1996b, 1997; Sacks et al., 1998) who used the laser-induced proton pulse technique for resolving the proton transfer reactions on the protein's surface. In these experiments a purple membrane suspension was subjected to rapid successive proton pulses, and the rate of proton transfer between the protein's surface and the pyranine anion was monitored with microsecond resolution. The rigorous analysis of the signals yielded a set of rate constants indicating that the BR state of the protein

is characterized by a proton-collecting antenna located on its cytoplasmic surface. The elements of the system consist of three carboxylates (D104, E161, and E234) that form a tight cluster with a rather high pK value (5.5) that reacts with free protons at a rate constant of $k = 5.5 \times 10^{10}$ M^{-1} s^{-1}. This rate constant is significantly larger than that of an isolated carboxylate on a low dielectric surface, and indicates a merging of the Coulomb cages of more than two carboxylates. The cluster is close enough to D36 and D38 to serve as a local proton reservoir that delivers the proton with a virtual second-order reaction of $k > 10^{10}$ (Sacks et al., 1998). As was revealed by the study of Hubbell and co-workers (Mollaaghababa et al., 2000) and Rödig and Siebert (1999), the M state of the protein exhibits a new organization of the surface groups. Thus, it is of interest to find out whether the proton collecting function of the surface is different in the M state.

For this purpose we used two mutants in the present study, D96N and the triple mutant (D96G/F171C/F219L). The first one can be readily pumped into the late M state (M_N) by constant illumination (Radionov and Kaulen 1997, 1999; Radionov et al., 1999; Zimanyi et al., 1992; Muneyuki et al., 1999; Subramaniam et al., 1999). The triple mutant has a lower tendency to accumulate in the M state due to changed rate constants of rise and decay (Tittor et al., 2002) and unless the actinic light is very intense, the protein retains its BR state of the chromophore, while its structure resembles the late M configuration (Subramaniam et al., 1999).

The measurements described in the present study indicate that the late M configuration of the protein exhibits a proton-collecting system that differs in its components but not in functionality from that observed for the BR state of the protein, and exhibits improved proton equilibration with the bulk.

MATERIALS AND METHODS

The kinetic measurements were carried out as detailed in Checover et al. (1997, 2001) and Nachliel et al. (1996b). The reaction mixture was constantly mixed by a small magnetic disk and its pH was monitored. In cases where the pH was drifting, small aliquots of HCl or NaOH were added to maintain the pH within ± 0.04 units at the initial value. During the kinetic measurements the D96N sample was maintained in the M state by continuous illumination by a focused beam of a slide projector (150 W) filtered by a cutoff filter ($\lambda \geq 520$ nm).

The sample was irradiated by the third harmonic frequency of an Nd/Yag laser $\lambda = 335$ nm 1.5–1.8 mJ/pulse 3 ns FWHM at a rate of 10 Hz. The probing light was the 458 nm band (for monitoring the pyranine) or the 528 nm band (for monitoring the photon-triggered M→BR transition) of a CW argon laser. The extinction coefficients were 24,000 and 37,000 M^{-1} cm^{-2}, respectively.

Preparation of the sample for measurement

The purple membranes were suspended in 30 ml unbuffered 150 mM NaCl solution and spun down by centrifugation. The process was repeated three

TABLE 1 Kinetic properties of the proton-binding sites of the BR state of the WT bacteriorhodopsin

Proton Binding Site	n^*	pK	$X+H^+$	$XH+D38$	$X+\phi O^-$
D38	1	6.5 ± 0.1	$0.4 \pm 0.1 \times 10^{10}$	—	$<10^8$
D36	1	4.5 ± 0.4	$1.0 \pm 0.1 \times 10^{10}$	$\geq 1 \times 10^{11}$	$<10^8$
COO^-_{cyt}	3	5.4 ± 0.1	$2.9 \pm 0.25 \times 10^{10}$	6×10^9	5.2 ± 10^9
COO^-_{ext}	1	5.1 ± 0.3	$0.5 \pm 0.3 \times 10^{10}$	—	$9 \pm 2 \times 10^9$

The listed values reconstruct 14 independent measurements carried out at varying pH values with 6.4 μM protein, 45.1 μM pyranine, and 150 mM NaCl. Data taken from Checover et al., 2001.

*Denotes the number of carboxylates having the same features.

times to remove all buffers from the reaction mixture. The final suspended membrane was supplemented by pyranine, placed in the measuring cuvette, and purged by water-saturated N_2 gas for 15 min before initiation of the experiment. The purging continued throughout the whole experimental period. A pyranine solution in 150 mM NaCl was treated by the same procedure, and through its kinetic analysis the residual content of dissolved CO_2 was determined. The same concentration of CO_2 was assumed to be present in the membrane suspension.

Analysis of the signal was carried out as described in Checover et al. (2001) and the kinetic parameters used to reconstruct the WT dynamics are given in Table 1.

RESULTS AND DISCUSSION

Kinetics of relaxation of the pyranine signals

The rate-limiting step of the D96N photocycle is the re-protonation of the Schiff base, leading to accumulation of the M state during continuous illumination. Time-resolved measurements, using either FTIR or spin-labeling techniques (Sasaki et al., 1992; Mollaaghababa et al., 2000, Rödig and Siebert, 1999) had indicated that the accumulated state of the protein is characterized by a special conformation that appears at a slower rate than the formation of the absorbance of the deprotonation Schiff base, thus a special conformation state had been assigned to the deprotonated

form accumulated under these conditions and is termed M_N. In the present study the accumulation of this state was ensured by illuminating the measuring cell by a green ($\lambda \geq$ 520 nm) light source, which caused a total bleaching of the 568 nm absorbance of the solution with subsequent accumulation of absorbance at 410 nm. As the kinetic measurements were carried out with unbuffered solution, it was readily noticed that, when the light was turned on, the solution exhibited a small but resistant acidification (0.1–0.05 pH unit) that was perfectly reversible when the light was turned off. Additional illumination with the probing light ($\lambda =$ 458 nm) did not affect the measured pH changes, indicating that the steady state of M-BR was not altered by the probing light.

Fig. 1 depicts three relaxation dynamics; the steepest one (labeled Py) was measured with pyranine dissolved in 150 mM NaCl and is characterized by a typical non-exponential relaxation curve. The initial phase is rapid, but after ~5–7 μs the reaction becomes much slower. The fast phase corresponds with the diffusion-controlled reaction between the pyranine anion and the free proton. The slower phase is due to the presence of a marginal concentration of bicarbonate that traps some of the released protons and transfers it to the pyranine anion in a collisional reaction. The curve labeled

FIGURE 1 The re-protonation kinetic of pyranine following pulse dissociation. The experiment were carried out as described in Methods. Curve Py was measured in the absence of any addition and corresponds with the re-protonation of the incremental pyranine anion generated by the photo dissociation of the dye. Curve D96N was measured under the same conditions in the presence of 6.3 μM of D96N that was irradiated by a focused beam of a 100 W lamp ($\lambda \geq$ 520 nm). Curve WT is the reconstruction of the WT protein, by the parameters listed in Table 1, under the precise experimental conditions of curve D96N. The inset depicts the regeneration dynamics of the BR initial state caused by the excitation of the M state chromophore by the laser pulse.
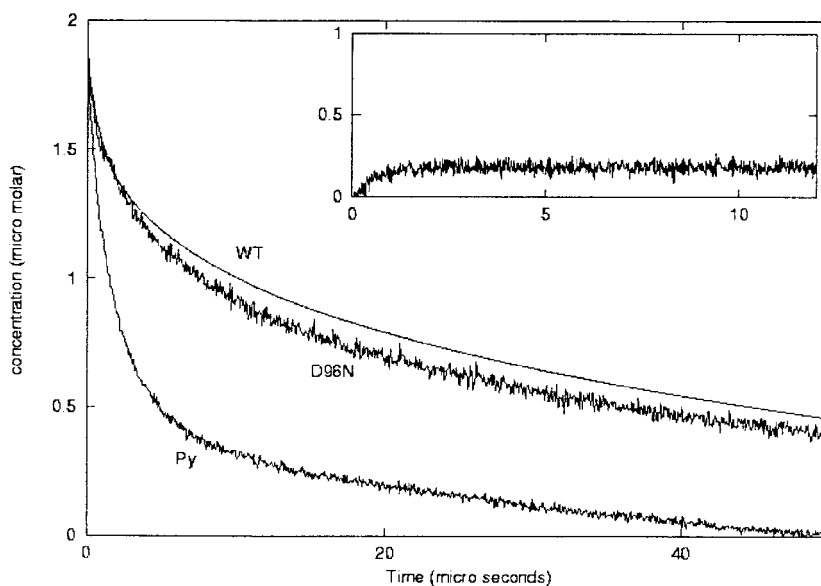
D96N was recorded in the same solution when supplemented by 7.3 μM of D96N mutated BR, which was converted to its M state by continuous illumination with green light. In this experiment the fast initial relaxation is almost missing, indicating that the proton-binding sites on the protein's surface effectively compete with the pyranine anion for the free proton. The slower phase corresponds with a mixed relaxation process where some of the protein-bound protons are released to the bulk by a dissociation reaction, while those attached to more basic proton binding sites are transferred to the dye by collisional proton transfer. For a detailed discussion of the mechanism see Checover et al. (2001). The curve labeled WT in Fig. 1 is a reconstruction of the pyranine signal using the same initial conditions and the parameters of the WT protein as listed in Table 1. It is clear that the retaining power of the BR state of the WT protein is significantly larger than that of the mutant.

The buffer capacity of a protein, determined by proton pulse measurements, is a function of the rate constant at which the surface proton binding sites react with free protons and their pK values, which are parameters determined by kinetic analysis. Because of the suspected difference between the buffer capacity of the WT and the mutated protein, it was imperative to determine the fraction of the BR initial state that was regenerated by photons absorbed by the M state (Haupts et al., 1996; Nagel et al., 1998; Oesterhelt et al., 1992; Tittor et al., 1994). Accordingly, the measurements were repeated using a measuring beam of $\lambda = 528$ nm, where the M-to-BR transition is characterized by a differential extinction coefficient of $\epsilon_{(BR-M)} = 33,700$ M^{-1} cm^{-1} that was calculated from the spectra of D96N (Miller and Oesterhelt, 1990). The recorded optical transient corresponded with 0.2 ± 0.04 μM of BR generated by the exciting laser pulse. In the range $6.7 \leq pH \leq 8.7$ the amount of the regenerated BR initial state was independent of the pre-pulse pH and of the presence of pyranine in the reaction mixture. This amount was $\sim$5% of the total protein concentration and constant for the BR concentrations used in the present experiment. The regeneration of the BR state had a rise time of $\tau \sim 300$–400 ns. A millisecond follow-up of the absorbance at 528 nm indicated that the increment of BR was constant in time and was removed from the observation space through dilution by the magnetic stirring. Because of the rather small increment of the BR initial state, its contribution to the buffer capacity of the system was not included in the kinetic analysis.

Kinetic analysis

The kinetic analysis of the signal consists of in silico reconstruction of the observed signal, where the input system is a set of coupled differential rate equations that corresponds to all proton transfer reactions proceeding in the reaction space. The rate constants of all proton transfer reactions are the adjustable parameters (Bransburg et al., 2000;

Checover et al., 2001; Gutman, 1984, 1986; Gutman and Nachliel, 1990; Gutman et al., 1985; Nachliel et al., 1996a).

The reconstruction of the measured signal was initially attempted by the parameters characterizing the WT protein whose cytoplasmic surface is characterized by four reactive elements (see Table 1): 1) the carboxylate of D38, which is partially exposed to the bulk and functions as the highest unoccupied proton binding site on the surface; 2) the carboxylate of residue D36, which is fully exposed to the bulk. Due to the proximity between the two residues (8.2 Å), D36 functions as an efficient proton donor to D38 with a very fast virtual second-order rate constant; 3) a cluster of three carboxylates (D104, E161, and E234 (Checover et al., 2001) that are close enough to function as a single, proton-attractive site that delivers protons to D36 and D38; 4) the fourth reactive element of the surface is a carboxylate located on the extracellular surface of the protein. Its contribution to the dynamics is rather small and will not be discussed in the present study. All other bulk-accessible residues of the protein make a negligible contribution to the dynamics, probably because their pK values are sufficiently low (pK $\leq$ 4). Such groups, once protonated, retain the bound proton for a time shorter than 1 μs (Gutman and Nachliel, 1990), which is too short to modulate the magnitude and shape of the pyranine re-protonation dynamics.

As seen in Fig. 1 curves D96N and WT, the solution suitable for the BR initial state of the WT protein was inadequate for the reconstruction of the transient measured with the D96N-M state protein. A further attempt to reconstruct the signals of the D96N-M state protein was based on the reaction pathway of the BR-WT system (cluster D36/D38), while modulating the pK values and the rate constants of the proton transfer reactions. As shown in Fig. 2 A, neither the modulation of the pK of the cluster, its rate of reaction with free proton (*panel B*), nor the pK of D38 (*panel C*) could retrace the signal measured with the D96N-M state. Modulation of the number of carboxylates (*panel D*) making the cluster was also insufficient for reconstructing the D96N-M state dynamics. These attempts indicate that a different pathway of proton transfer reactions characterizes the dynamics measured with the D96N-M state. Considering that the motion of the G and F helices affected the surface organization of the M structure, a new solution was looked for.

Instead of carrying out a de novo search over the whole parameter space, we adopted a strategy of correlating the kinetic analysis with the published structure of the cytoplasmic surface of the M state of the protein. Of the available M state PDB files (1C8S, 1DZE, 1F4Z, 1CWQ), we preferred that of Sass et al. (2000), as it reveals almost all residues on the cytoplasmic surface, except residues from 240 to 247 (at the tip of the C-terminal domain).

Fig. 3 depicts the cytoplasmic face of the M structure of bacteriorhodopsin as derived from the crystal structure. At present, as long as the solution structure of the protein is still

FIGURE 2 Comparison between the D96N-M state signal and reconstructed curves generated by the WT parameters. The experimental signal was measured at pH 6.97 and reconstructed by the reaction pathway of the BR initial state of the WT protein with modification of the parameters. (*A*) Reconstructed dynamics when the pK of the cytoplasmic cluster is varied from 6.0, 5.7, and 5.4 (lines 1, 2, and 3, respectively). In (*B*) the rate constant of protonation of the cytoplasmic cluster was varied from 10^{10} to 2×10^{10} and 6×10^{10} M^{-1} s^{-1}. In (*C*) the pK of the highest unoccupied base, identified with D38, was varied from 6, 6.5, and 7. (*D*) How the number of carboxylates in the cluster set consisting of one carboxylate (*line 1*), three carboxylates (*line 2*), and five carboxylates (*line 3*) affects the shape of the reconstruction curve.
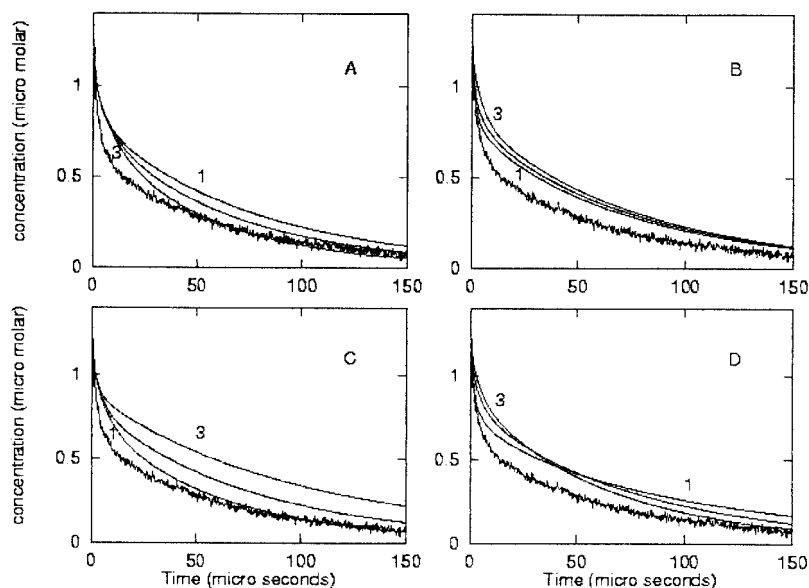
unresolved, we shall base all our evaluation on that structure. In this figure D38 is colored in yellow and its carboxylate carbon, like those of all other marked carboxylates, is emphasized in black. D38 is inserted in a hydrophobic pocket that is emphasized in white, and its oxygen atom of the carboxylate moiety is 4 Å from the nitrogen atom of
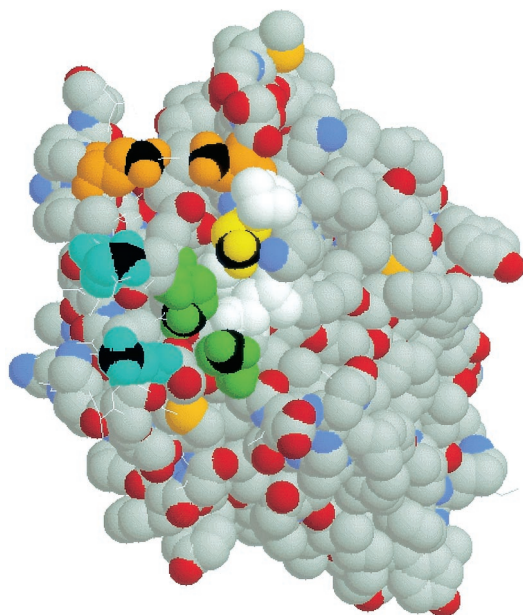

FIGURE 3 The cytoplasmic surface of the M state model of bacteriorhodopsin (PDB file 1CWQ, Chain B). Residue D38 is colored in yellow; D36 and D237 are in orange; D102 and E232 are in green, and residue E234 and E161 are in cyan. For clarity the carboxylate's carbon atom of these residues is marked in black. Residues P37 and F42 and l99 are colored in white. For the distance between the residues in the BR state and the M state, see Table 2.

K41 (~1 Å closer than in the BR state of the WT protein). This proximity might stabilize the structure through a salt bridge. There are two proton-conducting tracks leading toward D38. One pathway consists of D36, which is 8.2 Å from the carboxylate of D38 and is adjacent to the carboxylate of E237 (2.6 Å apart). The separation between the carboxylates along this pathway is comparable with the width of one or two solvation layers. Such proximity is suitable to sustain a fast proton transfer reaction, as was noticed between the proton binding sites of fluorescein (Sacks et al., 1998). The second proton-conducting track, colored in green, consists of D102 and E232. The D38-D102 separation (carboxylate to carboxylate) is 6.3 Å. The carboxylates of D102 and E232 are 4.8 Å apart. The cyan-colored carboxylates (E161 and E234) appear to form another proton-attractive pair that are 4.2 Å apart but are not well connected to D38. The distances between these residues in the BR state and the M state, based on PDB file 1cwq, is given in Table 2. Comparison to the compiled data indicates that in the M state the carboxylates are in a more condensed configuration, an arrangement that enhances the probability of efficient proton transfer between the nearby sites (Sacks et al., 1998).

The reconstruction of the transient measurements, recorded with the D96N-M state protein, was carried out in compliance with the structural features. The most basic unoccupied proton binding site of the protein, whose reaction with free pyranine is extremely slow, was identified as D38, confirming results of previous studies (Checover et al., 1997, 2001; Nachliel and Gutman, 1996; Nachliel et al., 1996b, 1997). The two proton conducting tracks, D102+E232 and D36+E237, were allowed to have a pK value that ranged from 4 to 7 and their rate constant of proton exchange with D38 was set to vary from 10^8 to 10^{12}.

TABLE 2 The distances between the carboxylates residues involved in the proton-collecting function of the cytoplasmic surface in its M state of bacteriorhodopsin

Residue Pair	M (Å)	BR (Å)
D36/D38	**8.2**	**6.9**
D36/E237	**2.6**	**4.4**
D38/E237	8.1	10.0
D96/D38	10.9	11.6
D102/D38	**6.3**	**7.7**
D102/D104	8.5	7.0
E161/E166	5.4	10.3
E161/E232	6.5	8.8
E161/E234	**4.2**	**6.2**
E166/E232	6.5	9.3
D102/E232	**4.8**	**4.0**
E234/D38	11.6	10.8
E234/E166	4.3	7.5
E234/E237	11.4	7.6

The values were measured from the structure of Sass et al. (2000; PDB entry 1cwq). Distances that are discussed in detail are marked in bold. The indicated distances are between carbon atoms of the carboxylates.

The upper limit corresponds with proton transfer between well-connected sites, where the donor and acceptor may share a common water molecule in their solvation shell. The lower value does not imply any connectivity between the reactants. The rate of the protonation of the two tracks by free protons was allowed to vary from 5×10^8 to 5×10^{10} $M^{-1} s^{-1}$, a range that extends from above the maximal rate according to the Debye-Smoluchowski equation, down to ~1% of this value. Within this parameter space we looked for a set of parameters that will reconstruct all experimental recordings with no systematic deviations.

The kinetic analysis of a complex system, such as a protein, necessitates that all protein molecules will be in the same conformation, and only one proton will probe the protein's surface. Under these restrictions, the response of the protein is stochastic; the initial state of all protein molecules is the same, and there is no cross-correlation between the molecules. Exposing a protein molecule to more than one proton implies that the first proton will affect the reactivity of the protein with the second. In the same sense, when the protein population exists in more than one state of protonation, there is a possibility that the analysis will yield average values, which are specific for the composition of the population at the pH of measurements. For

this reason the analysis is initiated by reconstructing the signals measured at the high end of the pH range, assuming that above pH 8 all surface carboxylates will be ionized while the more basic residues, like the lysine and tyrosine moieties, will be in their fully protonated state. Indeed, in the high range $6.9 \leq pH \leq 8.25$, a single set of parameters was obtained that accurately reconstructed all signals gathered in that range. On lowering the pH of the measurements, some of the carboxylates are protonated and the homogeneity of the protein population is lost. Indeed, below pH 6.9 the consistency of the solution was lost, suggesting that we have a mixture of states that varies their proportion with the pH. Therefore, no attempts were made to investigate the kinetics at pH values lower than 6.9.

The set of parameters that accurately reconstructed 25 independent experimental records, all measured in the pH range where the protein exists as one population, is given in Table 3, and the fitting of the curves is depicted in Fig. 4. The two panels depict the reconstructed dynamics at two extreme pH values. Fig. 4 *A* corresponds with a measurement carried out at pH 6.97, where the pyranine is below its pK value and most of it is in the *φ*OH state, ensuring a high yield of released protons. At this pH, the carboxylate of D38 is largely deprotonated and functions as the unoccupied proton-binding site on the protein with the highest pK. The experimental signals, together with the reconstructed curve, are presented at two levels of time resolution: 250 μs (*main panel*) and 50 μs (*inset*). Fig. 4 *B* depicts the reconstruction of the signal measured at pH 8.25, where the dissociation of the *φ*OH in the ground state lowers the magnitude of the perturbation and accelerates the relaxation due to the higher abundance of the pyranine anion. Accordingly, the signals differ in amplitude and relaxation time, yet both of them and 21 signals measured in the intermediate pH range and at different protein/pyranine ratios are reconstructed by the same set of parameters (Table 3).

The parameters listed in Table 3 compose the minimal system capable of reconstructing all experimental observations. A higher number of reactive residues will increase the complexity of the system with no gain in the accuracy of the reconstruction or understanding of the system.

The unoccupied proton-binding site with the highest pK has a value of 6.4; its rate constant for the reaction with free protons is ~10% of the rate of a diffusion-controlled reac-

TABLE 3 Kinetic parameters characterizing the proton transfer reactions on the cytoplasmic surface of bacteriorhodopsin in its M state

	*n**	pK	$X^- + H^+$	$XH + \phi O^-$	$XH + D38$	$XH + Track\ 1$
D38	1	6.4	$0.1 \pm 0.03 \times 10^{10}$	$k < 10^7$	—	—
Track 1	2	5.3	$2.5 \pm 0.4 \times 10^{10}$	$0.9 \pm 0.2 \times 10^{10}$	*$1 \pm 0.2 \times 10^{10}$*	NA
Track 2	2	4.8	$2.5 \pm 0.5 \times 10^{10}$	$0.9 \pm 0.25 \times 10^{10}$	*$2 \pm 0.2 \times 10^{10}$*	*1×10^9*
COO^-_{ext}	1	5.1	$0.5 \pm 0.1 \times 10^{10}$	$0.5 \pm 0.1 \times 10^{10}$	—	—

*Corresponds with the number of carboxylates that are characterized by the same parameters. The rate constants are given in $M^{-1} s^{-1}$ except for the virtual second-order reactions, which are printed in italics.

FIGURE 4 Reconstruction of the relaxation of the pyranine signals measured with D96N-M state at pH values where the kinetic parameters are still pH-independent. (*A*) The reconstruction at pH 6.97 in the time windows of 250 μs and 50 μs (*inset*). (*B*) The reconstruction of the signal, measured at pH 8.25.
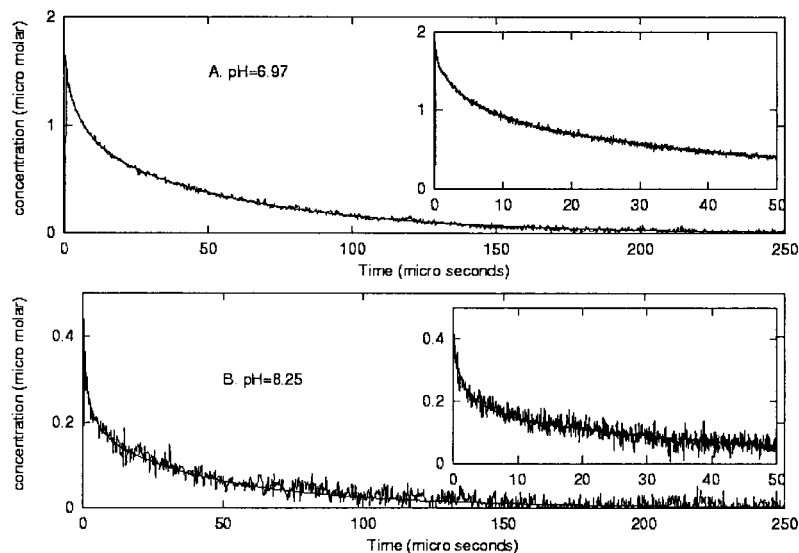
tion and it is practically inaccessible to pyranine anion. Based on these properties we identify it with D38. The other proton-binding sites are two pairs of carboxylates having pK values of 5.3 and 4.8, defined as tracks 1 and 2, respectively. Both tracks have comparable rate constants for reaction with free protons and pyranine anions, but differ in the rate constant for proton transfer to D38. According to the rate constants, track 2 is better-connected with D38, but considering the same minimal distance between D38 and D36 and D232, respectively, there is no way to identify the track with the residues.
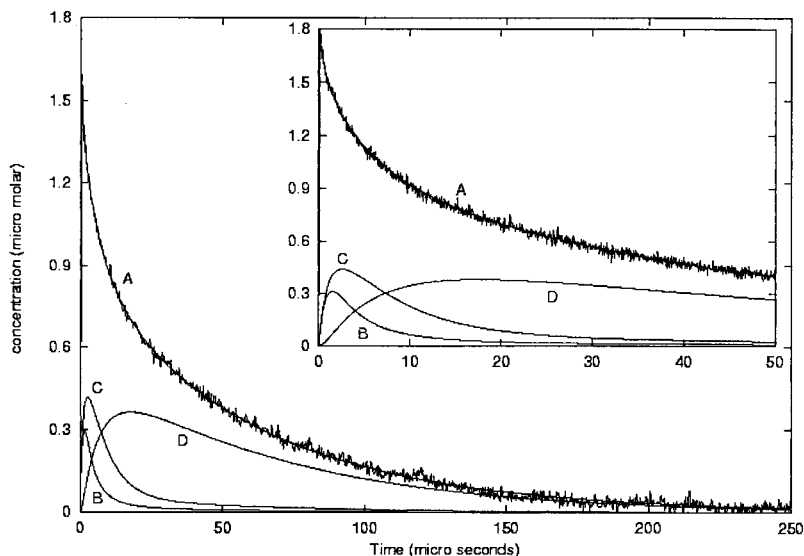
The mechanism of surface proton transfer

Fig. 5 depicts the reconstructed time evolution of the protonated state of the proton binding sites whose parameters are given in Table 3. Both tracks, 1 and 2, react with free protons at the same rate constants, yet as the rate of proton exchange between track 2 and D38 is faster than the other, and the ΔpK values also favor track 2 as a donor, the depletion of the protonated state of track 2 is faster and its maximal amplitude is smaller.

The accumulation of protons on track 1 has the same initial velocity, but its deprotonation is almost twice as slow. The combination of the two accessory systems leads to protonation of D38 within ~20 μs, even that by itself this residue is hardly accessible to the bulk; its rate of reaction with free proton is ~10% of the rate predicted by the Debye-Smoluchowski equation and pyranine hardly accepts protons from D38 (see Table 3). The limited access of pyranine to the opening of the proton-conducting channel also extends the dwell time of protons on D38 up to $\tau \sim 100$

FIGURE 5 Reconstructed time evolution of the protonated state of the proton binding sites ascribed to the D96N-M state protein. *Curve A* is the experimental signal together with the reconstructed pyranine dynamics. *Curves B* and *C* correspond with the transient protonation of tracks 2 and 1, respectively, and *curve D* is the protonation of D38. Please note that the rise of *curve D* is coupled with the decay of *curves B* and *C*. The inset depicts the dynamics when expanded for the first 50 μs.
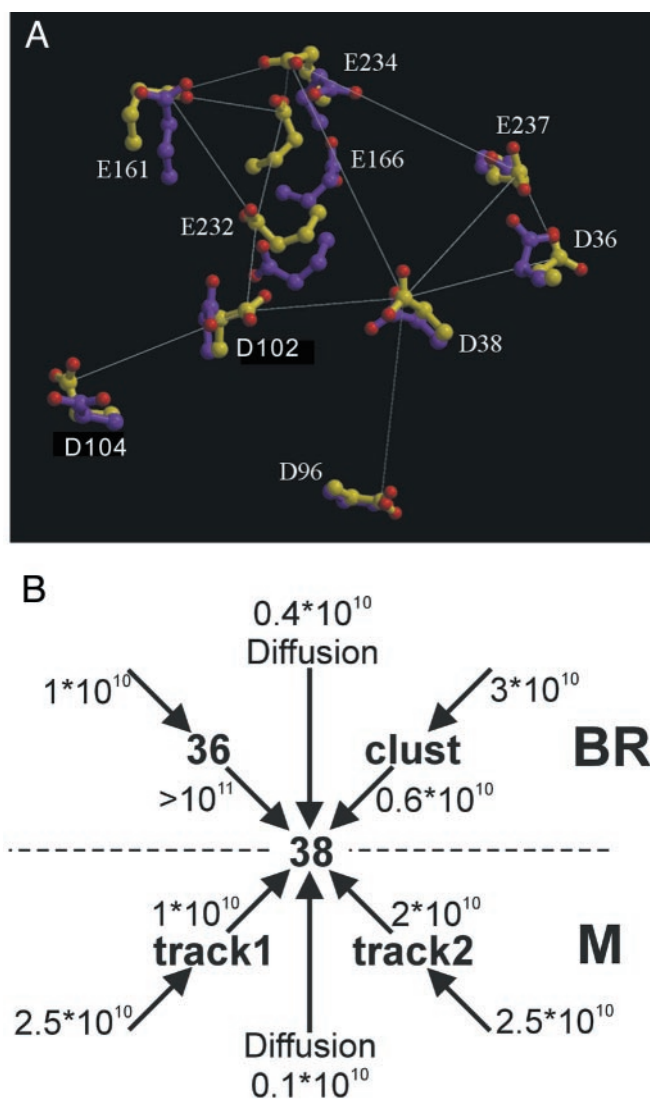
FIGURE 6 Surface proton transfer pathways in bacteriorhodopsin initial- and M-state. (*A*) Atomic model of the carboxylic side chains at the cytoplasmic surface of bacteriorhodopsin. The initial state is in purple; the M state, in green lines, indicates the distances given in Table 2. (*B*) Schematic representation of the proton conduction pathways in the initial and M states. The numbers at the arrows represent the rate constants and are given in $M^{-1} s^{-1}$.

μs. The combination of a fast protonation of D38 and limited accessibility to soluble proton acceptors ensures efficient delivery of protons to the proton-conducting channel. A scheme of this discussed proton transfer pathways is presented in Fig. 6.

The protonation dynamics of the triple mutant

The triple mutant (D96G/F171C/F219L; Subramaniam et al., 1999) is characterized by a ground state structure that resembles the late M state of the WT bacteriorhodopsin. The intensity of light source used in the present study did not produce an appreciable transient absorbance at 410 nm, and it was assumed that the protein remained mostly in its ground state. The triple mutant membranes were suspended in 150 mM NaCl and, in the presence of 23 μM pyranine, subjected to proton pulse experiments, but without background illumination. The transient formation of the pyranine anion, its subsequent re-protonation, and the reconstructed curves are depicted in Fig. 7.

The strategy of analysis was to start the process at high pH values and to proceed toward lower values until the pH independence of the parameters was lost. In the range $7.7 \leq pH \leq 8.1$, a single set of parameters (listed in Table 4) that fitted 14 independently measured signals was obtained. Below pH 7.7 the set of parameters became pH-dependent and continued to vary down to pH 6.2. Therefore, no attempt was made to analyze the variable range of the solution.

The pH-independent solution of the triple mutant system is similar in nature to that of the D96N-M state protein. There is one residue that functions as the most basic, unoccupied proton binding site, and this residue is poorly exposed to the bulk. Besides, there are two proton-conducting tracks leading to it. The difference between the triple mutant and D96N-M state is in the pK values and the rate constants of the proton transfer reactions. The pK of the most basic, unoccupied proton-binding site of the triple mutant is higher than that of the D96N-M state and the two tracks are more efficient. One is made of two carboxylates that are sufficiently close to form a common target. The second track is made of a cluster of three carboxylates that has even higher proton attractivity, both in pK and in rate of reaction with free proton. Thus, based on functional analysis, the proton-collecting features of the triple mutant seem to resemble those of the D96N-M state. Considering the experimental fact that the triple mutant exists as a mixture of all-*trans* and 13-*cis* (Tittor et al., 2002) a detailed structural evaluation of the parameters is premature.

CONCLUSIONS

The structure of two proteins, both considered as representative of the "late M state," has been analyzed (Luecke et al., 1999a; Sass et al., 2000; Subramaniam et al., 1999). In both cases we noticed that the protonation of the carboxylate identified as D38 proceeds through an indirect pathway. The residue itself is partially buried with a limited accessibility of bulk ions (both protons and the pyranine anion), and its protonation is mediated by a fast proton transfer from well-exposed carboxylates.

The proton-collecting antenna was first ascribed to the cytoplasmic surface of the BR (initial) state of the WT protein, but the participating residues, identified by extensive mutation analysis, are not those identified as the collecting elements in the late M structures. The structural rearrangements in the M state allow for a more efficient

FIGURE 7 Experimental signal of the triple mutant and its reconstructed dynamics. The measurements were carried out in unbuffered, 150 mM NaCl containing 3.5 μM protein, 15.3 μM pyranine at pH 7.86. *Curve A* depicts the experimental signal and its reconstruction; curves *B–D* reconstruct the transient protonation of track 1, track 2, and D38, respectively. The inset shows the same traces at higher time resolution.
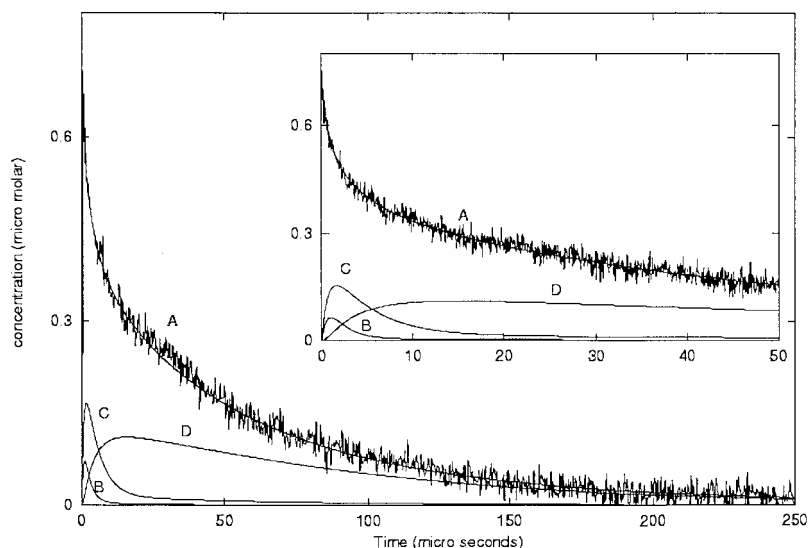
TABLE 4 Kinetic parameters characterizing the proton transfer reactions on the cytoplasmic surface of the triple mutant of bacteriorhodopsin

	$n*$	pK	$X+H^+$	$XH+\_O^-$	$XH+D38$
D38	1	6.9	0.1×10^{10}	$k < 10^7$	–
Track 1	2	4.9	$4.0 \pm 0.5 \times 10^{10}$	$8.5 \pm 0.5 \times 10^9$	*$2.0 \pm 0.5 \times 10^{10}$*
Track 2	3	5.6	$4.5 \pm 0.5 \times 10^{10}$	$8.5 \pm 0.5 \times 10^9$	*$2.5 \pm 0.5 \times 10^{10}$*
COO_{ext}^-	1	5.1	$0.5 \pm 0.1 \times 10^{10}$	$0.5 \pm 0.1 \times 10^{10}$	–

*Corresponds with the number of carboxylates that are characterized by the same parameters. The rate constants are given in $M^{-1}\,s^{-1}$ except for the virtual second-order reactions, which are printed in italics.

protonation by a factor of ~3 of the partially buried residue D38 at the entrance of the re-protonation channel of BR, which by all likelihood is the proton donor for D96.

REFERENCES

Bransburg, Z. S., O. Fried. Y. Marantz, E. Nachliel, and M. Gutman. 2000. Biophysical aspects of intra-protein proton transfer. *Biochim. Biophys. Acta.* 1458:120–134.

Brown, L. S., A. K. Dioumaev, R. Needleman, and J. K. Lanyi. 1998. Local-access model for proton transfer in bacteriorhodopsin. *Biochemistry.* 37:3982–3993.

Brown, L. S., J. Sasaki, H. Kandori, A. Maeda, R. Needleman, and J. K. Lanyi. 1995. Glutamic acid 204 is the terminal proton release group at the extracellular surface of bacteriorhodopsin. *J. Biol. Chem.* 270: 27122–27126.

Cao, Y., G. Varo, M. Chang, B. Ni, R. Needleman, and J. K. Lanyi. 1991. Water is required for proton transfer from aspartate-96 to the bacteriorhodopsin Schiff base. *Biochemistry.* 30:10972–10979.

Checover, S., Y. Marantz, E. Nachliel, M. Gutman, M. Pfeiffer, J. Tittor, D. Oesterhelt, and N. Dencher. 2001. Dynamics of the proton transfer reaction on the cytoplasmic surface of bacteriorhodopsin. *Biochemistry.* 40:4281–4292.

Checover, S., E. Nachliel, N. Dencher, and M. Gutman. 1997. Mechanism of proton entry into the cytoplasmic section of the proton-conducting channel of bacteriorhodopsin. *Biochemistry.* 36:13919–13928.

Chon, Y., J. Sasaki, H. Kandori, L. Brown, J. K. Lanyi, R. Needleman, and A. Maeda. 1996. Hydration of the counterion of the Schiff base in the chloride-transporting mutant of bacteriorhodopsin: FTIR and FT-Raman studies of the effects of anion binding when Asp85 is replaced with a neutral residue. *Biochemistry.* 35:14244–14250.

Dencher, N., H. Sass, and G. Büldt. 2000. Water and bacteriorhodopsin: structure, dynamics and function. *Biochim. Biophys. Acta.* 30:192–203.

Gutman, M. 1984. The pH jump: probing of macromolecules and solution by a laser-induced, ultrashort proton pulse—theory and application in biochemistry. *Met. Biochem. Anal.* 30:1–103.

Gutman, M. 1986. Application of the laser-induced proton pulse for measuring the protonation rate constants of specific sites on proteins and membranes. *Meth. Enzymol.* 127:522–538.

Gutman, M., and E. Nachliel. 1990. The dynamic aspects of proton transfer processes. *Biochim. Biophys. Acta.* 1015:391–414.

Gutman, M., E. Nachliel, and E. Gershon. 1985. Effect of buffer on kinetics of proton equilibration with a protonable group. *Biochemistry.* 24:2937–2941.

Hatanaka, M., J. Sasaki, H. Kandori, T. Ebrey, R. Needleman, J. K. Lanyi, and A. Maeda. 1996. Effects of arginine 82 on the interactions of internal water molecules in bacteriorhodopsin. *Biochemistry.* 35:6308–6312.

Haupts, U., E. Bamberg, and D. Oesterhelt. 1996. Different modes of proton translocation by sensory rhodopsin I. *EMBO J.* 15:1834–1841.

Haupts, U., J. Tittor, E. Bamberg, and D. Oesterhelt. 1997. General concept for ion translocation by halobacterial retinal proteins: the isomerization/switch/transfer (IST) model. *Biochemistry.* 36:2–7.

Heberle, J., and N. Dencher. 1992. Surface-bound optical probes monitor protein translocation and surface potential changes during the bacterio-rhodopsin photocycle. *Proc. Natl. Acad. Sci. U.S.A.* 89:5996–6000.

Heberle, J., J. Fitter, H. Sass, and G. Büldt. 2000. Bacteriorhodopsin: the functional details of a molecular machine are being resolved. *Biophys. Chem.* 85:229–248.

Heberle, J., D. Oesterhelt, and N. Dencher. 1993. Decoupling of photo-and proton cycle in the Asp85→Glu mutant of bacteriorhodopsin. *EMBO J.* 12:3721–3727.

Henderson, R., J. Baldwin, T. Ceska, F. Zemlin. E. Beckmann, and K. Downing. 1990. Model for the structure of bacteriorhodopsin based on high-resolution electron cryomicroscopy. *J. Mol. Biol.* 213:899–929.

Kandori, H., N. Kinoshita, Y. Yamazaki, A. Maeda, Y. Shichida, R. Needleman, J. K. Lanyi, M. Bizounok, J. Herzfeld, and J. Raap. 1999. Structural change of threonine 89 upon photoisomerization in bacterio-rhodopsin as revealed by polarized FTIR spectroscopy. *Biochemistry.* 38:9676–9683.

Koch, M., N. Dencher, D. Oesterhelt, H. Plöhn, G. Rapp, and G. Büldt. 1991. Time-resolved x-ray diffraction study of structural changes asso-ciated with the photocycle of bacteriorhodopsin. *EMBO J.* 10:521–526.

Lanyi, J. K. 1998. Understanding structure and function in the light-driven proton pump bacteriorhodopsin. *J. Struct. Biol.* 124:164–178.

Lanyi, J. K. 1999. Progress toward an explicit mechanistic model for the light-driven proton pump bacteriorhodopsin. *FEBS Lett.* 464:103–107.

Lanyi, J. K., and A. Pohorille. 2001. Proton pumps: mechanism of action and applications. *Trends Biotechnol.* 19:140–144.

Luecke, H., B. Schobert, T. Richter, J. Cartailler, and J. K. Lanyi. 1999a. Structural changes in bacteriorhodopsin during ion transport at 2 Ang-strom resolution. *Science.* 286:255–260.

Luecke, H., B. Schobert, T. Richter, J. Cartailler, and J. K. Lanyi. 1999b. Structure of bacteriorhodopsin at 1.55 Å resolution. *J. Mol. Biol.* 291: 899–911.

Miller, A., and D. Oesterhelt. 1990. Kinetic optimization of bacteriorho-dopsin by aspartic acid 96 as an internal proton donor. *Biochim. Biophys. Acta.* 1020:64–67.

Mollaaghababa, R., H. Steinhoff, W. Hubbell, and G. Khorana. 2000. Time-resolved site-directed spin-labeling studies of bacteriorhodopsin: loop-specific conformational changes in M. *Biochemistry.* 39: 1120–1127.

Mueller, D., G. Büldt, and A. Engel. 1995. Force-induced conformational change of bacteriorhodopsin. *J. Mol. Biol.* 249:239–243.

Muneyuki, E., C. Shibazaki, H. Ohtani, D. Okuno, M. Asaumi, and T. Mogi. 1999. Time-resolved measurements of photovoltage generation by bacteriorhodopsin and halorhodopsin adsorbed on a thin polymer film. *J. Biochem.* 125:270–276.

Nachliel, E., S. Checover, and H. Gutman. 1997. The role of the surface group in funneling of protons towards the protonic channel of bacterio-rhodopsin. *Solid State Ionics.* 97:75–82.

Nachliel, E., Y. Finkelstein, and M. Gutman. 1996a. The mechanism of monensin-mediated cation exchange based on real time measurements. *Biochim. Biophys. Acta.* 1285:131–145.

Nachliel, E., and M. Gutman. 1996. Quantitative evaluation of the dynam-ics of proton transfer from photoactivated bacteriorhodopsin to the bulk. *FEBS Lett.* 393:221–225.

Nachliel, E., H. Gutman, S. Kiryati, and N. Dencher. 1996b. Protonation dynamics of the extracellular and cytoplasmic surface of bacteriorho-dopsin in the purple membrane. *Proc. Natl. Acad. Sci. U.S.A.* 93: 10747–10752.

Nagel, G., B. Ketely, B. Möckel, G. Büldt, and E. Bamberg. 1998. Voltage dependence of proton pumping by bacteriorhodopsin is regulated by the voltage-sensitive ratio of M1 to M2. *Biophys. J.* 74:403–412.

Oesterhelt, D. 1998. The structure and mechanism of the family of retinal proteins from halophilic archea. *Curr. Opin. Struct. Biol.* 8:489–500.

Oesterhelt, D., J. Tittor, and E. Bamberg. 1992. A unifying concept for ion translocation by retinal proteins. *J. Bioenerg. Biomembr.* 24:181–191.

Oesterhelt, F., D. Oesterhelt, M. Pfeiffer, A. Engel, H. Gaub, and D. Müller. 2000. Unfolding pathways of individual bacteriorhodopsin. *Science.* 288:143–146.

Oka, T., H. Kamikubo, F. Tokunaga, J. K. Lanyi, R. Needleman, and M. Kataoka. 1999. Conformational change of helix G in the bacteriorho-dopsin photocycle: investigation with heavy atom labeling and x-ray diffraction. *Biophys. J.* 76:1018–1023.

Otto, H., T. Marti, M. Holz, T. Mogi, M. Lindau, G. Khorana, and M. Heyn. 1989. Aspartic acid 96 is the internal proton donor in the repro-tonation of the Schiff base of bacteriorhodopsin. *Proc. Natl. Acad. Sci. U.S.A.* 86:9228–9232.

Pebay-Peyroula, E., G. Rummel, J. Rosenbusch, and E. Landau. 1997. X-ray structure of bacteriorhodopsin at 2.5 Å from microcrystals grown in lipidic cubic phases. *Science.* 277:1676–1681.

Pfeiffer, M., T. Rink, K. Gerwert, D. Oesterhelt, and H. Steinhoff. 1999. Site-directed spin-labeling reveals the orientation of the amino acid side-chains in the E-F loop of bacteriorhodopsin. *J. Mol. Biol.* 287: 163–171.

Radionov, A., and A. Kaulen. 1997. Inhibition of the M1→M2 (M(closed)→M(open)) transition in the D96N mutant photocycle and its relation to the corresponding transition in the wild-type bacteriorhodop-sin. *FEBS Lett.* 409:137–140.

Radionov, A., and A. Kaulen. 1999. Two forms of N intermediate (N(open) and N(closed)) in the bacteriorhodopsin photocycle. *FEBS Lett.* 451: 147–151.

Radionov, A., V. Klyachko, and A. Kaulen. 1999. Formation of the M(N) (M(open)) intermediate in the wild-type bacteriorhodopsin photocycle is accompanied by an absorption spectrum shift to shorter wavelength like that in the mutant D96N bacteriorhodopsin photocycle. *Biochemistry (Mosc.).* 64:1210–1214.

Richter, T., R. Needleman, and J. K. Lanyi. 1996. Perturbed interaction between residues 85 and 204 in Tyr185→Phe and Asp85→Glu bacte-riorhodopsins. *Biophys. J.* 71:3392–3398.

Riesle, J., D. Oesterhelt, N. A. Dencher, and J. Heberle. 1998. D38 is an essential part of the proton translocation pathway in bacteriorhodopsin. *Biochemistry.* 35:6635–6643.

Rödig, C., and F. Siebert. 1999. Distortion of the L→M transition in the photocycle of the bacteriorhodopsin mutant D96N: a time resolved step-scan FTIR investigation. *FEBS Lett.* 445:14–18.

Royant, A., K. Edman, T. Ursby, E. Pebay-Peyroula, E. Landau, and R. Neutze. 2000. Helix deformation is coupled to vectorial proton transport in the photocycle of bacteriorhodopsin. *Nature.* 406:645–648.

Rüdiger, M., J. Tittor, K. Gerwert, and D. Oesterhelt. 1997. Reconstitution of bacteriorhodopsin from the apoprotein and retinal studied by Fourier-transform infrared spectroscopy. *Biochemistry.* 36:4867–4874.

Sacks, V., Y. Marantz, A. Aagaard, S. Checover, E. Nachliel, and M. Gutman. 1998. The dynamic feature of the proton collecting antenna of a protein surface. *Biochim. Biophys. Acta.* 1365:232–240.

Sasaki, J., Y. Shichida, J. K. Lanyi, and A. Maeda. 1992. Protein changes associated with reprotonation of the Schiff base in the photocycle of Asp96→Asn bacteriorhodopsin. The MN intermediate with unproto-nated Schiff base but N-like protein structure. *J. Biol. Chem.* 267: 20782–20786.

Sass, H., G. Büldt, R. Gessenich, D. Hehn, D. Neff, R. Schlesinger, J. Berendzen, and P. Ormos. 2000. Structural alterations for proton trans-location in the M state of wild-type bacteriorhodopsin. *Nature.* 406: 649–653.

Sass, H., R. Gessenich, M. Koch, D. Oesterhelt, N. Dencher, G. Büldt, and G. Rapp. 1998. Evidence for charge controlled conformational changes in the photocycle of bacteriorhodopsin. *Biophys. J.* 75:399–405.

Sass, H., I. Schachowa, G. Rapp, M. Koch, D. Oesterhelt, N. Dencher, and G. Büldt. 1997. The tertiary structural changes in bacteriorhodopsin occur between M states: x-ray diffraction and Fourier transform infrared spectroscopy. *EMBO J.* 16:1484–1491.

Steinhoff, H., M. Pfeiffer, T. Rink, O. Burlon, M. Kurz, J. Riesle, E. Heuberger, K. Gerwert, and D. Oesterhelt. 1999. Azide reduces the hydrophobic barrier of the bacteriorhodopsin proton channel. *Biophys. J.* 76:2702–2710.

Steinhoff, H., A. Savitsky, C. Wegener, M. Pfeiffer, M. Plato, and K. Möbius. 2000. High-field EPR studies of the structure and conforma-tional changes of site-directed spin labeled bacteriorhodopsin. *Biochim. Biophys. Acta.* 1457:253–262.

Subramaniam, S., M. Gerstein, D. Oesterhelt, and R. Henderson. 1993. Electron diffraction analysis of structural changes in the photocycle of bacteriorhodopsin. *EMBO J.* 12:1–8.

Subramaniam, S., M. Lindahl, P. Bullough, A. Faruqi, J. Tittor, D. Oesterhelt, L. Brown, J. K. Lanyi, and R. Henderson. 1999. Protein conformational changes in the bacteriorhodopsin photocycle. *J. Mol. Biol.* 287:145–161.

Tanio, M., S. Tuzi, S. Yamaguchi, R. Kawaminami, A. Naito, R. Needleman, J. K. Lanyi, and H. Saito. 1999. Conformational changes of bacteriorhodopsin along the proton-conduction chain as studied with (13)C NMR of (3(13)C)Ala.labeled protein:arg 82 may function as an information mediator. *Biophys. J.* 77:1577–1584.

Thorgeirsson, T., W. Xiao, L. Brown, R. Needleman, J. K. Lanyi, and Y. Shin. 1997. Transient channel-opening in bacteriorhodopsin: an EPR study. *J. Mol Biol.* 273:951–957.

Tittor, J., S. Paula, S. Subramaniam, J. Heberle, R. Henderson, and D. Oesterhelt. 2002. Proton translocation by bacteriorhodopsin in the absence of substantial conformational changes. *J. Mol. Biol.* 319:555–565.

Tittor, J., U. Schweiger, D. Oesterhelt, and E. Bamberg. 1994. Inversion of proton translocation in bacteriorhodopsin mutants D85N, D85T and D85,96N. *Biophys. J.* 67:1682–1690.

Varo, G., and J. K. Lanyi. 1990. Protonation and deprotonation of the M, N and O intermediates during the bacteriorhodopsin photocycle. *Biochemistry.* 29:6858–6865.

Varo, G., and J. K. Lanyi. 1991a. Kinetic and spectroscopic evidence for an irreversible step between deprotonation and reprotonation of the Schiff base in the bacteriorhodopsin photocycle. *Biochemistry.* 30:5008–5015.

Varo, G., and J. K. Lanyi. 1991b. Thermodynamics and energy coupling in the bacteriorhodopsin photocycle. *Biochemistry.* 30:5016–5022.

Varo, G., and J. K. Lanyi. 1995. Effects of the hydrostatic pressure on the kinetics reveal a volume increase during the bacteriorhodopsin photocycle. *Biochemistry.* 34:12161–12169.

Weik, M., G. Zaccai, N. Dencher, D. Oesterhelt, and T. Hauss. 1998. Structure and hydration of the M-state of the bacteriorhodopsin mutant D96N studied by neutron diffraction. *J. Mol. Biol.* 275:625–634.

Xiao, W., L. Brown, R. Needleman, J. K. Lanyi, and Y. Shin. 2000. Light-induced rotation of a transmembrane alpha-helix in bacteriorhodopsin. *J. Mol. Biol.* 304:715–721.

Zimanyi, L., Y. Cao, M. Chang, B. Ni, R. Needleman, and J. K. Lanyi. 1992. The two consecutive M substates in the photocycle of bacteriorhodopsin are affected specifically by the D85N and D96N residue replacements. *Photochem. Photobiol.* 56:1049–1055.

Zscherp, C., R. Schlesinger, J. Tittor, D. Oesterhelt, and J. Heberle. 1999. In situ determination of transient pKa changes if internal amino acids of bacteriorhodopsin by using time-resolved attenuated total reflection Fourier-transformed infrared spectroscopy. *Proc. Natl. Acad. Sci. U.S.A.* 96:5498–5503.